J. Fluid Mech. (2008), *vol.* 601, *pp.* 63–84.
doi:10.1017/S0022112008000451 Printed in the United Kingdom

Effects of matrix viscoelasticity on viscous and viscoelastic drop deformation in a shear flow

NISHITH AGGARWAL AND KAUSIK SARKAR

Department of Mechanical Engineering, University of Delaware, Newark, DE-19716, USA
sarkar@udel.edu

(Received 25 July 2007 and in revised form 27 December 2007)

The deformation of a Newtonian/viscoelastic drop suspended in a viscoelastic fluid is investigated using a three-dimensional front-tracking finite-difference method. The viscoelasticity is modelled using the Oldroyd-B constitutive equation. Matrix viscoelasticity affects the drop deformation and the inclination angle with the flow direction. Numerical predictions of these quantities are compared with previous experimental measurements using Boger fluids. The elastic and viscous stresses at the interface, polymer orientation, and the elastic and viscous forces in the domain are carefully investigated as they affect the drop response. Significant change in the drop inclination with increasing viscoelasticity is observed; this is explained in terms of the first normal stress difference. A non-monotonic change – a decrease followed by an increase – in the steady-state drop deformation is observed with increasing Deborah number (De) and explained in terms of the competition between increased localized polymer stretching at the drop tips and the decreased viscous stretching due to change in drop orientation angle. The transient drop orientation angle is found to evolve on the polymer relaxation time scale for high De. The breakup of a viscous drop in a viscoelastic matrix is inhibited for small De, and promoted at higher De. Polymeric to total viscosity ratio β was seen to affect the result through the combined parameter βDe indicating a dominant role of the first normal stress difference. A viscoelastic drop in a viscoelastic matrix with matched relaxation time experiences less deformation compared to the case when one of the phases is viscous; but the inclination angle assumes an intermediate value between two extreme cases. Increased drop phase viscoelasticity compared to matrix phase leads to decreased deformation.

1. Introduction

Understanding the dynamics of an emulsion's microstructure is critical for designing them with macroscopic properties tuned to particular applications. For emulsions with a globular morphology, deformation, breakup and coalescence of dispersed drops determine the emulsion rheology (Tucker & Moldenaers 2002; Li & Sarkar 2005*b*; Aggarwal & Sarkar 2007*a*, *b*). Single drop deformation and breakup in a Newtonian system and their implications on rheology have been studied extensively (for a review see Rallison 1984; Stone 1994; Tucker & Moldenaers 2002). However, investigation of the corresponding viscoelastic system has been rare. Consequently, there is a lack of understanding of the behaviours of such systems. We reported a numerical investigation of the deformation and breakup of an Oldroyd-B drop in a Newtonian matrix (O/N) (Aggarwal & Sarkar 2007*a*), as well as the rheology of an

emulsion of such drops (Aggarwal & Sarkar 2007*b*). Here, we investigate the reverse system (N/O) of a Newtonian drop in an Oldroyd-B matrix as well as the case when both phases are viscoelastic (O/O).

In the O/N system, viscoelasticity results in a decreased drop deformation owing to the first normal stress inside the drop (deformation D shows a scaling $D \sim D_{De=0}(1 - Ca De)$ with Capillary Ca and Deborah De numbers for small Ca and De, Aggarwal & Sarkar 2007*a*). There is a transient overshoot in deformation owing to the finite time needed for the viscoelastic stress to develop. Aggarwal & Sarkar (2007*a*) provided an ordinary differential equation model that explains the behaviour.

On the other hand, there have been conflicting theories and experimental reports about the effects of matrix elasticity on drop deformation. In one of the earliest experiments on the effects of viscoelasticity on drop deformation, Flummerfelt (1972) found that for a Newtonian drop sheared in a viscoelastic matrix, the critical shear rate $\dot{\gamma}_c$ for initiation of breakup increases with increasing matrix elasticity, indicating an inhibiting effect of viscoelasticity. Tagvac (1972) found the matrix elasticity to have a stabilizing effect on a drop at low viscosity ratios, but an opposite effect at high viscosity ratios. Elmendorp & Maalcke (1985) performed experiments on systems where either the drop or the matrix phase was viscoelastic, and found that the drop elasticity inhibited drop deformation, whereas matrix viscoelasticity enhanced it in simple shear. Mighri *et al.* (1997, 1998) studied systems with Boger fluids, which have constant shear viscosity, and observed that drop elasticity decreases deformation whereas matrix elasticity increases it. They further noted that for elasticity ratio (ratio of the relaxation of the drop phase to that of the matrix phase) $k \leqslant 0.37$, the deformation of an elastic drop in an elastic matrix is larger than the Newtonian (N/N) case. However, for $k > 0.37$, an elastic drop in an elastic matrix deforms less than in the N/N case. In contrast, Sibillo, Simeone & Guido (2004) found that the matrix elasticity stabilized a Newtonian drop in a simple shear.

Vanoene (1972) created a simple model where the surface tension was modified to account for the differences in first normal stresses in the two fluids, which predicts that higher normal stresses in the drop (matrix) phase stabilizes (destabilizes) the drop. However, the model is over-simplified in that it assumes a parabolic flow to compute the stresses, which might not be valid in general. Greco (2002) obtained a perturbative solution to $O(Ca^2)$ of a system of second-order fluids. This solution is used to obtain two slightly different modifications of the Maffetone–Minale's (1998) phenomenological model by Maffetone & Greco (2004) and Minale (2004). Greco's theory compares well with experiments by Guido, Simeone & Greco (2003) performed with a Newtonian drop in Boger fluids. They showed significant deviation from Newtonian behaviour (at small deformation) only in the orientation of the drop and not in the deformation. The orientation was found to be independent of the second normal stress differences of the matrix fluid at this order. The modified phenomenological model due to Maffetone and Greco also agrees well with experimental results (Maffettone & Greco 2004; Maffettone *et al.* 2005). Maffetone & Greco (2004) also predicted N_2 of the matrix to have a significant stabilizing effect on the drop against breakup. Minale's (2004) modification, besides being for viscoelasticity, was also designed to capture the divergence of Ca_{cr} with $\lambda \to 0$ for a Newtonian system. It predicts opposing effects of N_1 and N_2 on drop deformation for the viscoelastic matrix – Newtonian drop system. Minale chose a non-zero value N_2 to show a quantitative match with Guido *et al.*'s (2003) results. It should be pointed out that the second-order fluid used in Greco's model and therefore by other similar models, although valid for slow flows might not match with rate type equations such

as Oldroyd-B, especially for multiphase flow problems such as the one considered here.

Computational study of the viscoelastic single-drop problem has mostly been restricted to two-dimensional systems (Toose, Geurts & Kuerten 1995; Chinyoka *et al.* 2005; Yue *et al.* 2005*a*, *b*) or axisymmetric (Ramaswamy & Leal 1999*a*, *b*; Hooper *et al.* 2001) using rate type constitutive equations such as Oldroyd-B and FENE-CR. Khismatullin, Renardy & Renardy (2006) presented a three-dimensional study concentrating primarily on the implementation of the numerical method. Yue *et al.* (2005*a*, *b*) observed non-monotonic deformation for Newtonian drops in viscoelastic systems with increasing Deborah numbers, which might explain the apparent contradiction in recent literature regarding the effect of matrix viscoelasticity on drop deformation. However, their study is limited by the two-dimensional nature of their computations. Furthermore, although drop inclination angle is shown to be affected much more than deformation (Greco 2002; Guido *et al.* 2003; Maffettone & Greco 2004) it has not been given much attention in the numerical investigations. In the current study, we also see that the inclination angle plays a decisive role in the drop dynamics.

We present a full three-dimensional simulation of the deformation of a Newtonian and Oldroyd-B drop in an Oldroyd-B matrix. Oldroyd-B is one of the simplest materially frame-indifferent constitutive equations with a single relaxation time; it has a shear independent viscosity, a positive first normal stress and a zero second normal stress in steady shear. It has also been an equation of choice of recent numerical investigations (Hooper *et al.* 2001; Chinyoka *et al.* 2005; Yue *et al.* 2005*a*, *b*; Khismatullin *et al.* 2006; Aggarwal & Sarkar 2007*a*, *b*). As with the O/N system, we did not observe any numerical difficulties associated with the Oldroyd-B constitutive relation within the range of Deborah number studied. Section 2 describes the mathematical formulation of the problem. In § 3, we present a brief description of the numerical implementation using a three-dimensional finite-difference front-tracking algorithm. For details on the numerical implementation, see Aggarwal & Sarkar (2007*a*). Section 4 presents the results of our investigation of the small-Reynolds-number case ($Re = 0.1$). We compare with experimental observations and discuss the numerical results in the context of the previous numerical studies.

2. Mathematical formulation

This section follows closely the presentation in Aggarwal & Sarkar (2007*a*, *b*); it is presented here for the sake of completeness. The flow of the droplet matrix system is governed by the momentum conservation equation:

$$\frac{\partial(\rho \boldsymbol{u})}{\partial t} + \nabla\cdot(\rho \boldsymbol{u}\boldsymbol{u}) = \nabla\cdot\boldsymbol{\tau} - \int_{\partial B} \mathrm{d}\boldsymbol{x}_B \kappa \boldsymbol{n} \Gamma \delta(\boldsymbol{x} - \boldsymbol{x}_B), \tag{1}$$

in the entire domain. Γ is the interfacial tension (constant), ∂B represents the surface of the drop consisting of the points $\boldsymbol{x}_B$, κ the local curvature, $\boldsymbol{n}$ the outward normal, and $\delta(\boldsymbol{x} - \boldsymbol{x}_B)$ is the three-dimensional Dirac delta function. We represent the interfacial tension force as a singular body force in anticipation of the numerical (front-tracking) implementation. $\boldsymbol{\tau}$ is the total stress tensor given by:

$$\boldsymbol{\tau} = -p\boldsymbol{I} + \boldsymbol{T}^p + \boldsymbol{T}^v, \quad \boldsymbol{T}^v = \mu_s \boldsymbol{D}, \tag{2}$$

where p is the pressure, μ_s is the solvent viscosity and $\boldsymbol{D} = (\nabla\boldsymbol{u}) + (\nabla\boldsymbol{u})^T$ is the strain rate tensor. $\boldsymbol{T}^p$ is the extra stress (also referred to as polymer stress or viscoelastic

stress) due to the presence of the polymer. We use the Oldroyd-B constitutive equation for $\boldsymbol{T}^p$:

$$\lambda \overset{\nabla}{\boldsymbol{T}}^p + \boldsymbol{T}^p = \mu_p \boldsymbol{D}, \tag{3}$$

where μ_p is the polymeric viscosity, λ is the relaxation time ($\lambda = 0$ in the Newtonian component inside), and $\overset{\nabla}{\boldsymbol{T}}$ is the upper convected time derivative defined as:

$$\overset{\nabla}{\boldsymbol{T}}^p = \frac{\partial \boldsymbol{T}^p}{\partial t} + \boldsymbol{u} \cdot \nabla \boldsymbol{T}^p - (\nabla \boldsymbol{u}) \boldsymbol{T}^p - \boldsymbol{T}^p (\nabla \boldsymbol{u})^T. \tag{4}$$

The superscript T represents the transpose. The fluid is considered to be incompressible in both phases:

$$\nabla \cdot \boldsymbol{u} = \boldsymbol{0}. \tag{5}$$

The Oldroyd-B fluid does not show shear thinning effects. Shear flow of an Oldroyd-B fluid gives rise to a first normal stress difference, $N_1 = 2\mu_p \dot{\gamma}^2 \lambda$ and shear stress $T^p_{xy} = \mu_p \dot{\gamma}$ ($\dot{\gamma}$ is the shear) (see the Appendix).

3. Numerical implementation

The drop is placed in a computational domain with periodic boundary conditions in the x- (flow) and z- (vorticity) directions. Velocities are specified at the upper and lower plates in the y-direction to impose a simple shear of magnitude $\dot{\gamma}$. Boundary conditions on the extra stresses must be specified at the domain boundary. The hyperbolic Oldroyd-B constitutive equation requires only the inflow boundary conditions. Initially, a spherical drop of radius a is placed at the centre of the computational domain. At $t = 0$, the flow is started by the motion of the plates.

We use a front-tracking finite-difference method (Unverdi & Tryggvason 1992; Tryggvason *et al.* 1998, 2001; Sarkar & Schowalter 2000, 2001; Li & Sarkar 2005*a*). The drop-matrix two-phase system with different properties (density, viscosity, relaxation time) across a sharp drop boundary is transformed into a single-phase system with properties varying smoothly over a few computational grid points (here $\sim 4\Delta x$). The system therefore has the same equation everywhere, e.g. the same Oldroyd-B equation for polymeric stresses even in the Newtonian phase, with relaxation time $\lambda = 0$ (Sarkar & Schowalter 2000). In front tracking, the smoothed representations of the properties are found by solving a Poisson equation for the indicator function, which is zero outside and unity inside (Unverdi & Tryggvason 1992). Apart form a regular three-dimensional Cartesian grid in the entire domain, the moving interface (front) is separately discretized using triangular elements. The front is used in determining the properties. Once the smoothly varying property fields are attained, (1) is solved by a finite-difference method to obtain the velocities at the Cartesian grid points. The interface evolution is described by the nodal (triangle vertices) velocity on the front obtained by interpolation. For this interpolation as well as those involved in representing the singular terms in the Poisson equation and in (1) owing to the surface tension, a smoothed surrogate of the delta function (Peskin 1977) is used. An adaptive regridding scheme is used to prevent excessive distortion of the front elements. A novel analytic algorithm has been developed for the viscoelastic extensions of the front-tracking method, which automatically splits the viscous and the viscoelastic parts of the stress (Sarkar & Schowalter 2000; Aggarwal & Sarkar 2007*a*). Further details of the numerical implementation can be found in Aggarwal & Sarkar (2007*a*).

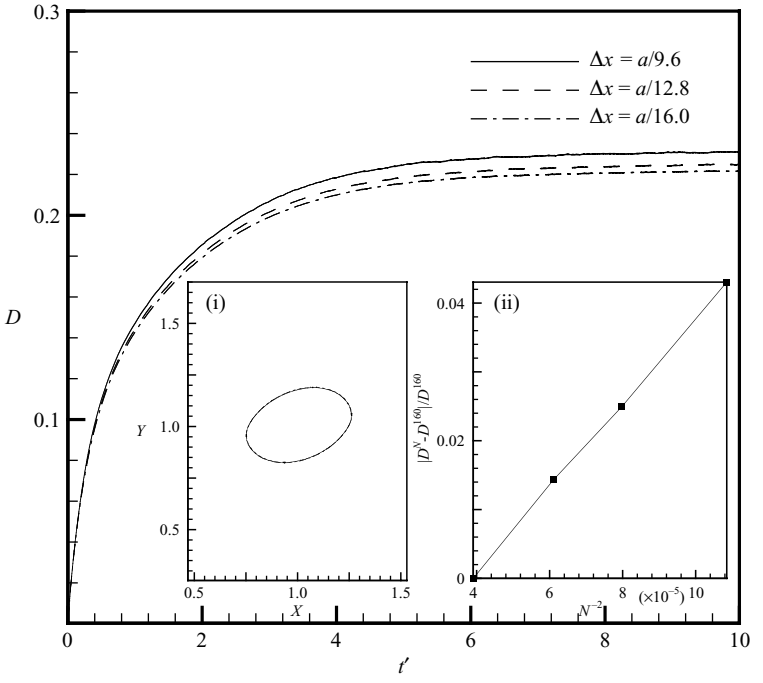

FIGURE 1. Convergence study – D *vs.* t' for $Ca = 0.2$ and $De = 1.5$ at different grid resolutions. Inset shows (i) convergence in computed steady-state drop shapes for the different resolutions, (ii) convergence in D value with increasing grid resolution. N is the number of grid points in the x-direction of the domain.

4. Results

We use the initial drop radius a and $\dot{\gamma}^{-1}$ as the length and time scales to define the various non-dimensional parameters governing the problem: Reynolds number $Re = \rho_m a^2 \dot{\gamma}/\mu_m$, capillary number $Ca = \mu_m a \dot{\gamma}/\Gamma$, Deborah number $De = \lambda \dot{\gamma}$, viscosity ratio $\lambda_\mu = \mu_d/\mu_m$, density ratio $\lambda_\rho = \rho_d/\rho_m$ and $\beta = \mu_p/\mu_m$ – the ratio of the polymeric to the total matrix viscosity (most results are for a Newtonian drop in an Oldroyd matrix (N/O), except when we briefly considered the O/O system). Subscripts m and d correspond to the matrix and the dispersed phase, respectively. For brevity, we restrict ourselves to cases with $\lambda_\rho = \lambda_\mu = 1$. We fix $Re = 0.1$ representing a low-Reynolds-number case. The governing non-dimensional parameters for the problem are then Ca, De and β. We have fixed $\beta = 0.5$ for all our results, unless specifically mentioned otherwise.

We have carefully established convergence of the viscoelastic algorithm in our previous paper for the O/N case (Aggarwal & Sarkar 2007*a*). In figure 1, we plot Taylor's (1932) deformation parameter $D = (L - B)/(L + B)$ at successively finer grid resolutions for $Ca = 0.2$ and a moderate value of $De = 1.5$ for the N/O system. We see small differences in the steady-state D values. However, no significant change is observed in the drop shapes for the different resolutions. In the inset, the error in deformation (relative to the highest resolution $160 \times 160 \times 80$ considered) for different discretization shows a quadratic convergence with the grid level. We choose a resolution of $\Delta x = \Delta y = \Delta z = a/9.6$ and time step $\Delta t = 0.005\dot{\gamma}^{-1}$ for our study. We use a domain size of $L_x = L_y = 2L_z = 10a$ (with $96 \times 96 \times 48$ grid points) as in our

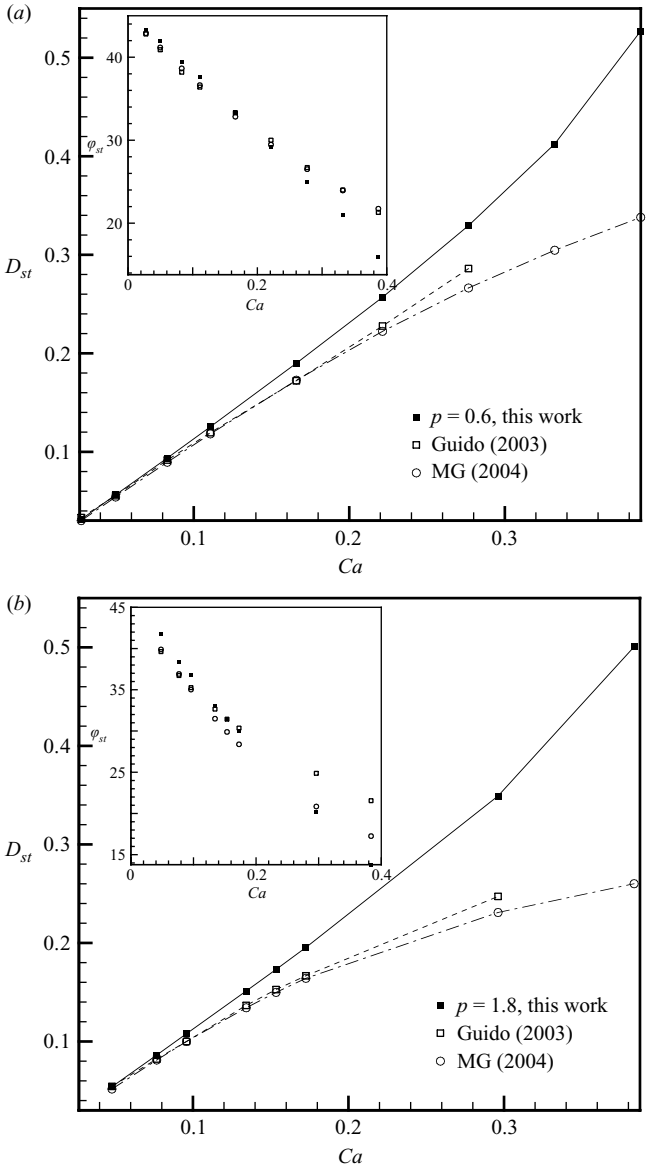

FIGURE 2. Comparison of steady-state drop response predictions with experimental results from Guido *et al.* (2003) and analytical predictions of Maffetone & Greco (2004). Drop deformation D_{st} and drop inclination angle φ_{st} (inset), for (*a*) $p = 0.6$ and (*b*) $p = 1.8$.

previous study. The adequacy of this domain size has been carefully established, but not presented here (see Aggarwal & Sarkar 2007*a* for the O/N case).

5. Comparison with experiments

In figure 2, we compare our steady-state numerical predictions of deformation D_{st} and inclination angle φ_{st} with results from the experimental work of Guido *et al.* (2003) and predictions of the phenomenological model of Maffetone & Greco (2004) (indicated by Guido (2003) and MG (2004) in the figures). The comparisons

are for elasticity parameter $p = De/Ca = 0.6$ and 1.8 (De and Ca are not varied independently in the experiments). The D_{st} values (figure 2) compare well with previous results for small shear rates; $D_{st} \sim Ca$ curves seem to diverge at higher shear rates. The comparison for $p = 0.6$ is much better than for $p = 1.8$. Our numerical predictions for D_{st} are consistently larger than both the experimental results and the model predictions. Comparison of φ_{st} shown in the insets matches well with the experimental results for small shear rates (up to $Ca \sim 0.2$). Again, the comparison is much better for $p = 0.6$. The disparity in the comparison at high shear rates and high elasticity parameter can be ascribed to the inability of the Oldroyd-B constitutive equation in representing the experimental fluid used by Guido *et al.* (2003). Moreover, our computations have been performed for equal contributions from solvent and polymeric viscosities to the total viscosity of the viscoelastic phase, i.e. $\beta = 0.5$. Variations with β are significant (Aggarwal & Sarkar 2007*a*) and could well result in a better fit with the experimental results. This study is, however, not undertaken. The comparison for φ_{st} is much better than that for D_{st}. It has been noted previously that the presence of second normal stresses differences N_2 in the matrix can significantly alter drop deformation both qualitatively and quantitatively (Levitt, Macosko & Rearson 1996; Hobbie & Migler 1999; Minale 2004), whereas Greco's analysis (2002) shows that the orientation angle is not significantly altered by N_2. An Oldroyd-B constitutive equation shows $N_2 = 0$ in simple shear flows and is thus incapable of capturing effects that are due to a finite N_2 of the matrix fluid. Minale (2004) used a finite value of N_2 to match with experimental results of Guido *et al.* (2003).

6. Transient deformation and orientation angle

In figures 3(*a*), 3(*b*) and 3(*c*) we plot the transient evolution of the three drop axes L, B and W for $Ca = 0.3$ with varying De. The drop axes lengths evolve monotonically to a steady-state value except for slight non-monotonicity at $De = 1$. All the three drop axes show non-monotonic trends in steady-state elongation with increasing elasticity. The steady state L decreases first with De, followed by an increase. B continues to increase (even though the deformation D decreases in figure 3*d*), and starts decreasing only for $De > 1.5$. The axis length along the vorticity direction W shows slight non-monotonicity, following trends similar to the primary axis L. The reversal in trends for the different drop axes does not occur at the same De, suggesting that the effects of viscoelasticity could be localized, affecting different regions of the drop interface differently.

In figure 3(*d*), we look at the evolution of the drop deformation parameter$D$. The transient deformation monotonically increases to a steady-state value for all values of De except for $De = 1$, where we see a slight overshoot. The steady-state deformation value shows a non-monotonic trend with De as seen for the three drop axes. With increasing elasticity, the initial drop deformation consistently slows down because the viscoelastic components of the stresses in the matrix grow as $T_{xx} = 2\mu_p \dot{\gamma}^2 \lambda\{1 - e^{-t/\lambda}(1 + t/\lambda)\}$ and $T_{xy} = \mu_p \dot{\gamma}(1 - e^{-t/\lambda})$, i.e. exponentially with a time scale λ for T_{xy} (or slower for T_{xx}) (see the Appendix). Accordingly, in the inset of figure 3(*d*) we show a magnified plot of the initial evolution. Note that the T_{xx} and T_{xy} expressions above are calculated for a system with initially fully developed shear flow, but zero initial extra stresses (as appropriate in a Stokes flow). Accordingly, for figures in the inset, here the simulations are also performed with such an initial condition. At small time t' the limiting case of $De \to \infty$ is the viscous case with the

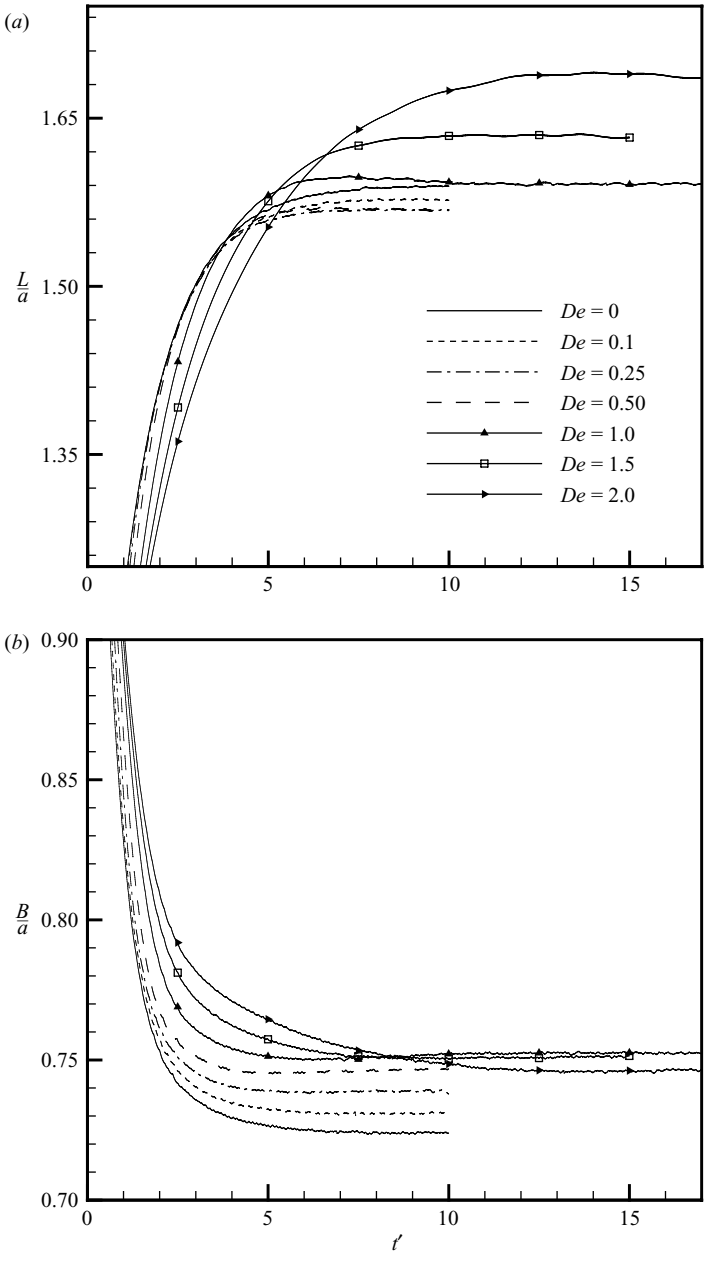

FIGURE 3(*a*, *b*). For caption see facing page.

matrix viscosity half the drop viscosity (Toose *et al.* 1995), because only the viscous stress becomes active in the viscoelastic matrix with matched total viscosities and $\beta = 0.5$.

Similar to the case of a viscoelastic drop in a Newtonian matrix (Yue *et al.* 2005*a*; Aggarwal & Sarkar 2007). Yue *et al.* (2005*a*) observed significant overshoot in the transient deformation of a Newtonian drop–viscoelastic matrix system, for intermediate Deborah numbers. Yue *et al.* (2005*a*) attributed the overshoot to the competition between the capillary and relaxation time scales – the fact that for

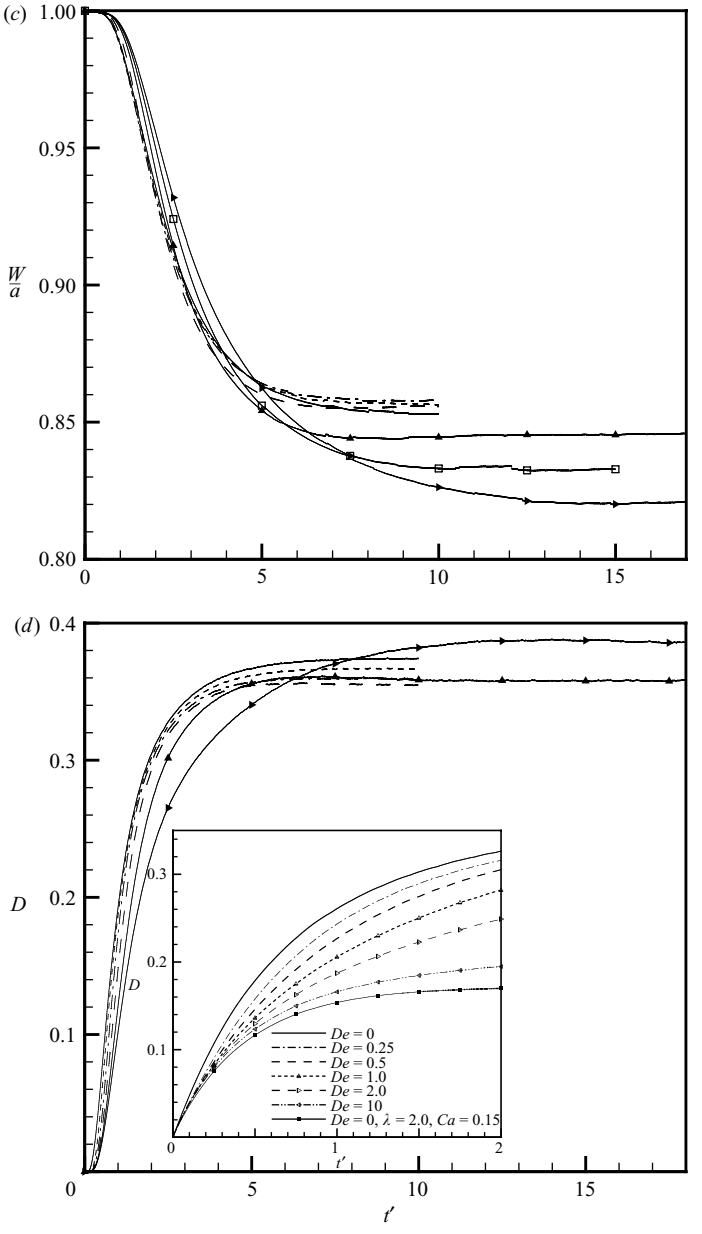

FIGURE 3. Transient drop evolution parameters plotted against non-dimensional time t' (*a*) Drop axes length L, (*b*) B, (*c*) W and (*d*) drop deformation parameter D for $Ca = 0.3$ and varying De. Inset for (*d*) shows the initial transient evolution of D. Curve legends are the same as in (*a*).

small De the viscoelasticity of the matrix inhibits drop deformation (also shown in a later section of this paper) and the viscoelastic stresses develop with a finite relaxation time scale. However, we do not see any significant overshoot except for systems with viscosity ratio $\lambda_\mu = \mu_d/\mu_m > 1$. For $\lambda_\mu = \mu_d/\mu_m > 1$, even a viscous system shows overshoot and oscillation in steady shear (Cox 1969). Note that the matrix viscoelasticity besides possibly inhibiting the drop deformation also retards

the development of the flow stress that stretches the drop. Therefore, the net result is a subtle balance of various effects. Maffettone *et al.* (2005) experimentally observed an overshoot in transient deformation of viscosity-matched Newtonian drop-viscoelastic matrix systems at high shear rates (see their figure 2). An overshoot, albeit less than that, was observed in the experiments, was also predicted by the phenomenological theory of Maffettone & Greco (2004). However Minale's (2004) model does not predict any appreciable overshoot. The three-dimensional VOF simulations of Newtonian drop deformation in viscoelastic matrix, using an Oldroyd-B matrix fluid (Khismatullin *et al.* 2006) also did not predict any overshoot (see their figure 11) for exactly the same parameter values used in experiments.

Next we look at the transient evolution of the drop inclination angle $\varphi(t)$ that the major drop axis L makes with the positive x-direction. For small deformation of viscosity-matched fully Newtonian systems, the orientation angle of a drop evolves on a capillary time scale (Torza, Mason & Cox 1972) and settles to a steady-state value. As the drop deforms, it experiences greater torque which aligns it towards a smaller inclination angle. This behaviour is also observed numerically. To illustrate this point, we plot the scaled transient deformation angle $\bar{\varphi} = (\varphi - \varphi_{st})/(45^\circ - \varphi_{st})$ *vs.* t' for fully viscous systems at different capillary numbers (figure 4*a*). Here, φ_{st} is the long-time steady value of the angle which decreases with Ca, and $t' = \dot{\gamma} t$ is the non-dimensional time. We also plot in the inset the parameter $\bar{\varphi}$ as a function of t'/Ca. The $\bar{\varphi}$ curves for different values of Ca overlap on scaling the independent variable with Ca, indicating its development with the capillary time scale. For a viscoelastic system, there is an additional time scale λ associated with polymer stress growth in the matrix. This effectively changes the evolution time for the inclination angle. In figure 4(*b*), we plot $\bar{\varphi}$ as a function of t' for $De = 2$. We see that the transient curves even for different Ca overlap with small disparity at this De, indicating that unlike the viscous case, the rate of change in the inclination angle is not governed by the capillary time scale. The transient evolution is governed by the polymer relaxation time. A similar collapse of curves for similarly scaled deformation $\bar{D}$ is not observed at high De. In the inset of the figure 4(*b*), the evolution of φ for different values of De at $Ca = 0.3$ shows an increased alignment of the drop with the flow at steady state with increased matrix viscoelasticity.

7. Steady-state deformation and inclination angle

The steady-state inclination angle φ_{st} is plotted as a function of De for different capillary numbers (figure 5*a*). In conformity with previous investigations (Guido *et al.* 2003; Chinyoka *et al.* 2005; Yue *et al.* 2005*b*), we see a significant decrease in the drop inclination angle with increasing matrix viscoelasticity. $\varphi_{st} \sim De$ curves are very similar for different Ca values, i.e. the rate of decrease of φ_{st} with De is not strongly dependent on the parameter Ca. Note that for an O/N system, Aggarwal & Sarkar (2007*a*) found that the inclination increased with drop phase viscoelasticity (the effect in O/N is much smaller). Agreement with the well-known second-order analytical result for the inclination angle in fully Newtonian systems $\varphi = \pi/4 - (2\lambda_\mu + 3)(19\lambda_\mu + 16)/80(\lambda_\mu + 1)Ca$, due to Chaffey & Brenner (1967), is also shown in the figure (indicated by CB (1967)). For viscosity-matched Newtonian systems, a more deformed drop (high Ca) experiences greater torque which aligns it towards the flow direction. For a viscoelastic fluid in shear, the direction of the principal stress component (of total stress) does not overlap with the principal strain direction (45° from the flow direction), because of the presence of the first normal stress difference N_1 in the matrix. With increasing relaxation time λ (i.e. increasing

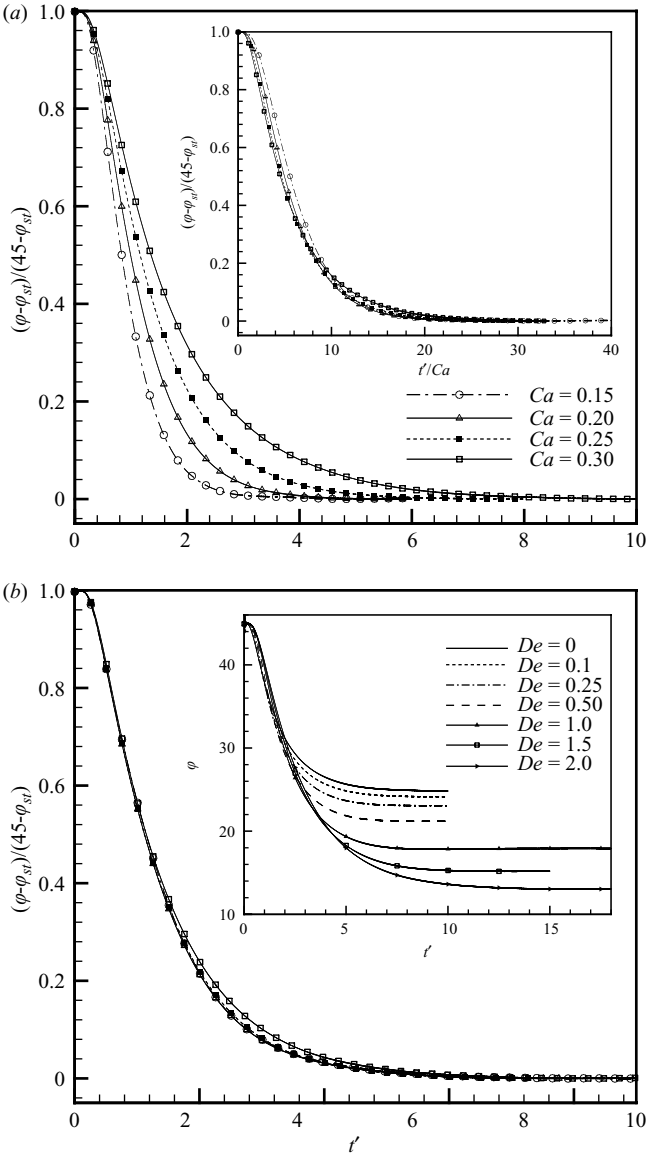

FIGURE 4. (*a*) Scaled inclination angle $\bar{\varphi}$ *vs.* non-dimensional time t' for $De = 0$. Inset shows $\bar{\varphi}$ plotted as a function of t'/Ca. (*b*) $\bar{\varphi}$ *vs.* t' for $De = 2$. Curve legends are the same as in (*a*). Inset shows transient drop inclination angle φ for different De at $Ca = 0.3$.

De), the dominant eigenvalue of the total stress tensor (tensile stress) aligns away from the principal extensional direction and towards the flow direction. This provides for an additional torque to the deforming drop, which decreases the orientation angle.

In figures 5(*b*), 5(*c*) and 5(*d*) we look at the steady-state deformation curves (deformation parameter D_{st}, and steady state axes lengths L, B and W) as a function of the Deborah number. The L, B and W curves are for two different capillary numbers. The drop deformation D_{st} does not change significantly within the range of our study. This was also observed in the experiments by Guido *et al.* (2003) and predicted by the second-order theory of Greco (2002) for small deformations and

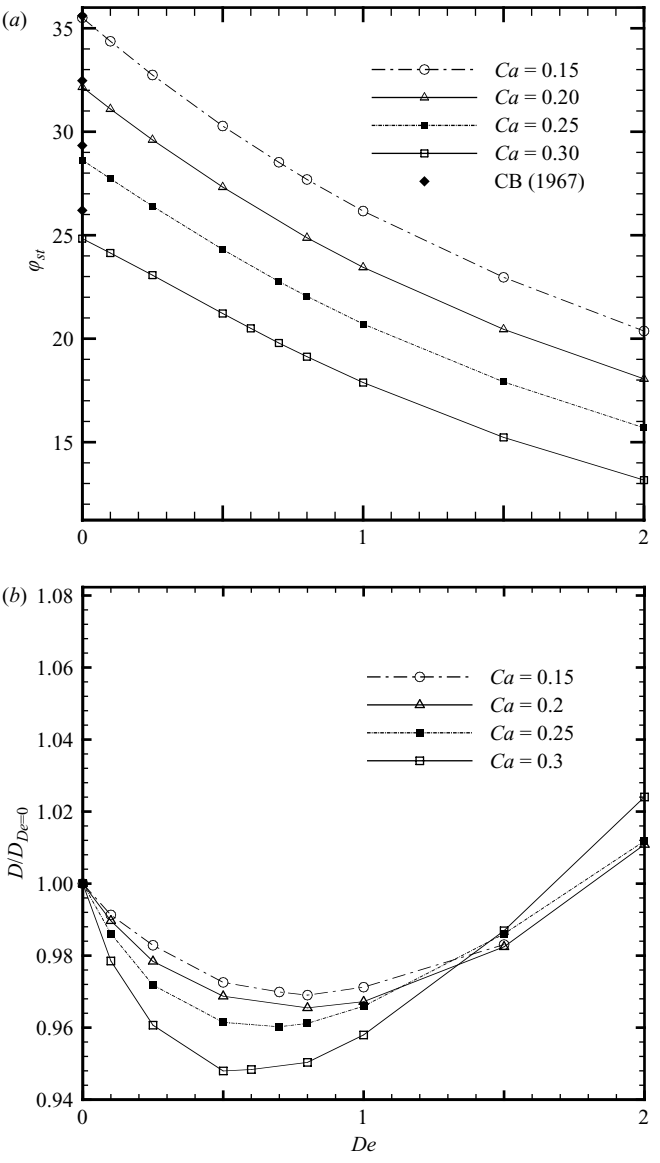

FIGURE 5(*a*, *b*). For caption see facing page.

$p \sim O(1)$. The $D_{st} \sim De$ curve is non-monotonic with an initial decrease (the initial decrease being larger for larger Ca) followed by an increase as is also seen from the transient deformation curves (figure 3*d*). The non-monotonicity of the $D_{st} \sim De$ curve was also observed in the two-dimensional study by Yue *et al.* (2005*b*). On the other hand, such non-monotonicity was not observed in experiments; neither is it predicted by analytical theories (Greco 2002; Maffettone & Greco 2004; Minale 2004). However, it should be noted that the experiments were performed for small elasticity parameter $p = De/Ca$ which restricts their $De \sim 0.6$. To understand better the reason for non-monotonicity, we carefully examine the individual axes lengths for two different values of Ca in figures 5(*c*) and 5(*d*). The initial decrease in the D_{st} is primarily due to the increase in the B axis length. This increase is arguably due to

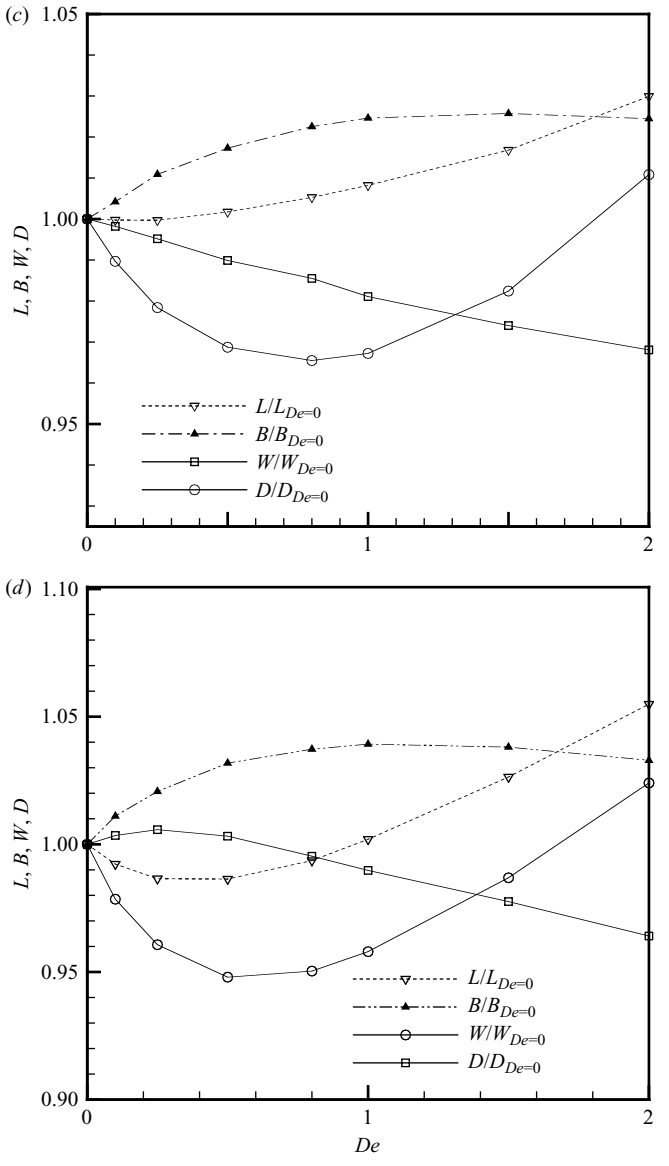

FIGURE 5. (*a*) Steady-state drop inclination angle φ_{st} varying with De for different Ca. (*b*) Steady-state drop deformation D_{st} (normalized against the value for $De = 0$) varying with De. Steady-state drop axes length L, B, W and deformation parameter D (normalized with $De = 0$ values) for (*c*) $Ca = 0.2$ and (*d*) $Ca = 0.3$.

the decrease in the orientation angle. A drop aligned away from the extensional axis, experiences lesser shearing force, and as a result, the drop deformation decreases. A similar decrease in overall deformation and L is expected because of the drop alignment.

In zero-vorticity linear flows such as the uniaxial and planar extensional flows, viscoelasticity of the matrix fluid is observed to increase the drop deformation monotonically (Mighri *et al.* 1997; Ramaswamy & Leal 1999*a*; Hooper *et al.* 2001). Tretheway & Leal (2001) concluded that the stagnation points at the tips of the drop

cause the extension of polymer chains, resulting in the formation of pointed ends, increased deformation and a decrease in the critical capillary number required to burst the drop. In a sheared system, the flow near the drop tips is locally extensional and we expect a similar extension of the polymer chains at that location. This would tend to increase drop deformation competing with the decreasing effects due to drop inclination away form the extension axis. Moreover, this should be a localized effect that primarily increases deformation at the tips and hence results only in an increase in the L axis length. Indeed, the L axis length increases monotonically for $Ca = 0.2$ (figure 5c) and shows only a slight decrease followed by an increase for $Ca = 0.3$ (figure 5d).

Following Yue *et al.* (2005*b*) and Aggarwal & Sarkar (2007*a*), we plot viscous and viscoelastic stresses along the circumference of the drop (in the central plane of the drop i.e. $z = L_z/2$) as a function of the angular position ϕ measured anticlockwise from the positive x-direction, for different De at $Ca = 0.3$. In figures 6(a) and 6(b) we plot the viscous and viscoelastic stress normal to the interface i.e. $T_{nn} = \boldsymbol{n} \cdot T \cdot \boldsymbol{n}$, where $\boldsymbol{n}$ is the normal vector to the drop interface. With increasing elasticity, the magnitude of the tensile viscous stress T^v_{nn} decreases in magnitude; the stress peaks shift consistently towards lower angular positions. This is due to the orientation of the drop away from the imposed flow's extensional direction. Also, the weakly compressive stress at the drop equator decreases in magnitude slightly. Both these observations indicate a decrease in the deforming viscous forces. The magnitude of the viscoelastic normal stress T^p_{nn} increases quite significantly, from being approximately equal to T^v_{nn} at small $De = 0.1$. This increase is local and primarily at the drop tips. A look at the primary orientation of the polymer molecules (primary eigen-direction of the conformation tensor $\boldsymbol{A} = (\lambda/\mu_p)\boldsymbol{T}^p + \boldsymbol{I}$ in the matrix for a representative case $Ca = 0.3$ and $De = 1$, in figure 7(a), indicates that the polymer molecules are indeed normal to the drop interface near the tips; stretching of the polymer molecules is a maximum here. This observation is in conformity with the observations of Pilapakkam & Singh (2001) but at variance with that of Yue *et al.* (2005*b*). Yue *et al.* observed the maximum stretching of the polymer molecules at the drop equator. We believe that a local extensional flow near the drop tips gives rise to large velocity gradients, thus locally increasing the stretching of the polymer molecules significantly.

Ramaswamy & Leal (1999*a*, *b*) pointed out that viscoelasticity could affect drop deformation through a change in both the balance of stresses normal to the drop interface and by inducing a change in the flow. In uniaxial extensional flows, the viscoelastic stresses at the interface cause a reduction in drop deformation and the curvature at the drop tips. However, a change in the flow, induced by the viscoelastic stresses resulted in an increased drop deformation. The final drop shape was a balance of the two opposing effects. In a shear flow, drop viscoelasticity has been found to cause little flow modification (Yue *et al.* 2005*b*; Aggarwal & Sarkar 2007*a*). Flow modification due to viscoelasticity can happen only through viscoelastic stress gradients. In figure 7(b) we look at the vector plot of the force due to the viscoelastic stresses, $\nabla \cdot \boldsymbol{T}^p$ in the matrix. It is evident that even at a small $De = 0.1$ (where we see a decreased deformation from the Newtonian value), the viscoelastic force tends to increase L and decrease B, i.e. increase the deformation. A similar plot for the viscous force $\nabla \cdot (\mu_s \nabla \boldsymbol{u})$ (not shown here for brevity), as expected, reveals also its tendency to enhance deformation. Steady state represents a balance between the viscous and viscoelastic forces trying to stretch the drop and the surface tension force trying to resist it. The reduction in viscous stretching owing to increased alignment at low De plays a crucial role in decreasing deformation from its Newtonian value. Note also that the magnitude of the viscoelastic force at the drop tips is significantly higher than that at the equator. This explains why B decreases almost monotonically because

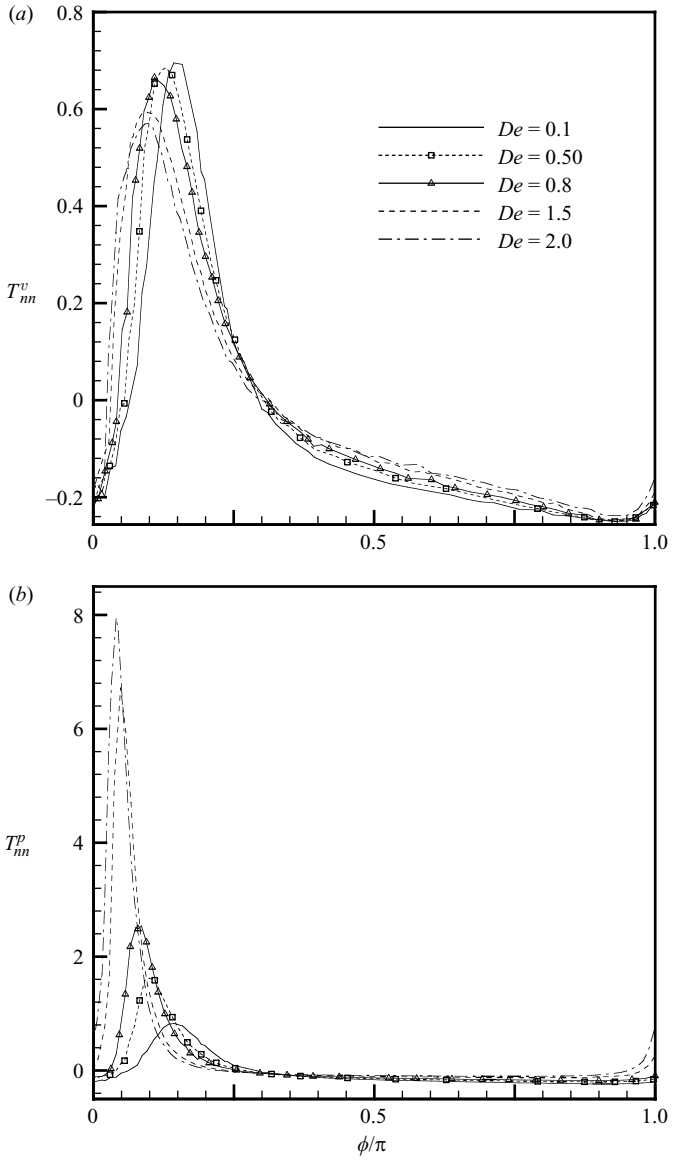

FIGURE 6. Stresses along the circumference of the drop in the central flow plane plotted as a function of the angular position ($\phi = 0$ coincides with x-axis) for $Ca = 0.3$ and varying De. (a) Viscous normal stresses T^v_{nn} and (b) viscoelastic normal stresses T^p_{nn}. Curve legends are the same as in (a).

of the alignment of the drop with the flow direction (decreased viscous stress), and L changes non-monotonically (decreasing viscous stress but increasing viscoelastic stress) with De for $Ca = 0.3$.

8. Large deformation and breakup

Finally, we look briefly at the effect of matrix viscoelasticity for large deformations (at $Ca = 0.4$). In figure 8, we plot the transient deformation measure L/a; the

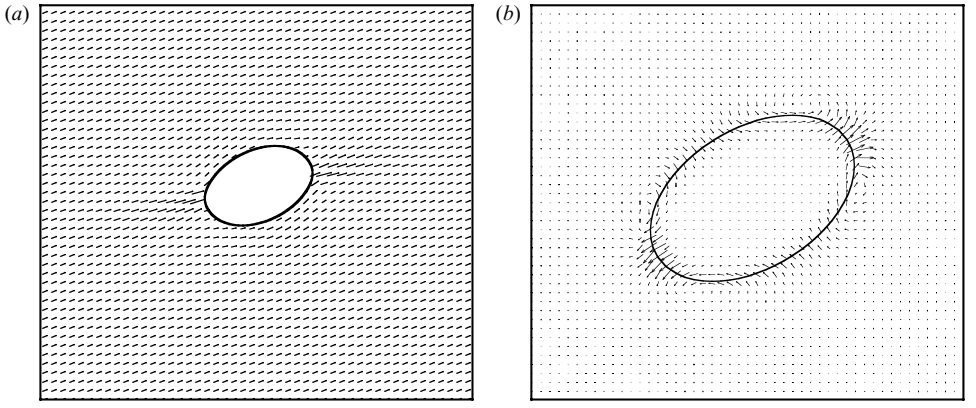

FIGURE 7. (*a*) Dominant orientation of polymer molecules for $Ca = 0.3$ and $De = 1$ in the central flow plane (*b*) Viscoelastic force field $\nabla \cdot \boldsymbol{T}^p$ for $Ca = 0.2$ and $De = 0.1$.

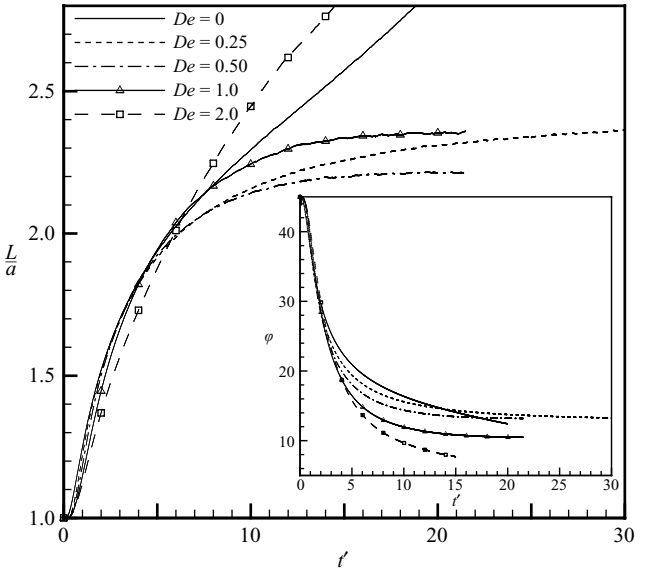

FIGURE 8. Transient drop deformation L/a predictions for parameter set close to the critical case, $Ca = 0.4$ and varying De.

inset shows the transient drop inclination angle. For $Ca = 0.4$ and $De = 0$, the fully Newtonian system is supercritical and results in an unbounded drop. For $De = 0.25$, the drop elongation process is slowed down as the drop quickly becomes aligned with the flow, but the drop eventually breaks. For still higher De (0.5 and 1.0), we see bounded drop deformations. Even though for $De = 1.0$ drop deformation is more than that at $De = 0.5$, there still exists a steady shape. Matrix phase viscoelasticity is seen to stabilize elongated drops in this small range of De. However, on further increasing $De(= 2)$ we see an unbounded drop deformation because the viscoelastic stresses are very strong and breakup the drop. In this way, the breakup behaviour mimics that of bounded deformation, in that smaller viscoelasticity inhibits drop breakup, but higher

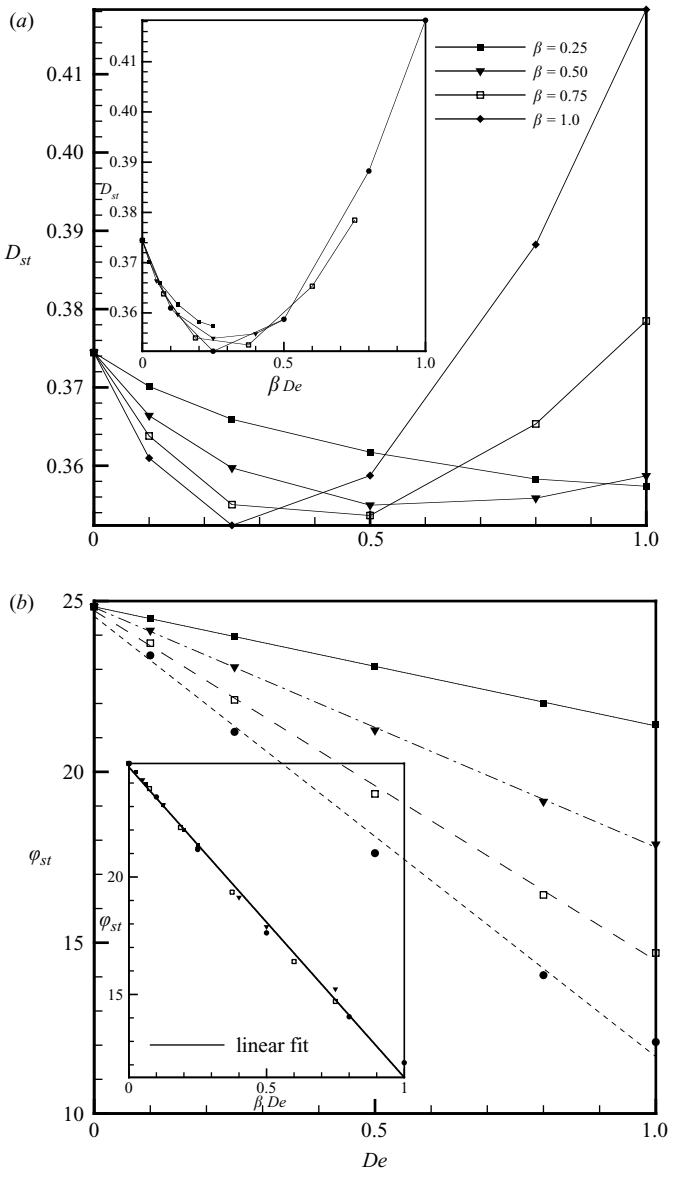

FIGURE 9. Steady-state drop response predictions for $Ca = 0.3$ and varying β values. (*a*) Drop deformation D_{st} (*b*) drop inclination angle φ_{st}. Insets show the dependent variables plotted against βDe. Curve legends are the same as in (*a*).

viscoelasticity enhances. The complete breakup process is slow and therefore involves lengthy computations beyond our current computational capabilities.

9. Effects of β variation

All the results presented so far are for a fixed value of $\beta = 0.5$. Variations with β amount to an increase in the contribution of the polymeric viscosity in the viscoelastic phase. Enhanced viscoelastic effects are thus expected for high β values. We plot in figures 9(*a*) and 9(*b*) the steady-state drop response varying with De, for $Ca = 0.3$

and different β values. The non-monotonic change in steady-state drop deformation (figure 9*a*) is seen for all β values. The change in trend for smaller β values is seen at higher De. On scaling the independent variable with β (shown in the inset) the initial descending parts of the curves collapse, indicating a βDe scaling. We attribute the decrease in deformation to alignment of the drop away from the principal extensional direction. In figure 9(*b*), we plot the steady-state inclination angle of the drop *vs.* De for varying β. An increase in viscoelastic effects owing to increase in β causes the angle to decrease more sharply with De. This decrease is linear in De. On scaling the x-axis with β (plotted in the inset) the change in angle is clearly seen to vary as βDe. The variation with βDe indicates the effect of the first normal stress difference in a steady shear $N_1 = 2\mu_p \dot{\gamma}^2 \lambda$, which when non-dimensionalized by $\mu_m \dot{\gamma}$ becomes $N_1 = 2\beta De$.

10. Elastic drop in an elastic matrix

The effect of drop viscoelasticity in shear flows has been studied and detailed in several previous investigations (Pillapakkam & Singh 2001; Yue *et al.* 2005*b*; Aggarwal & Sarkar 2007*a*). Elasticity of the drop phase results in an inhibition of the deformation (an attendant increasing alignment with the extensional axis is also observed). This effect is limited and saturates at high De. Here, we briefly consider both phases being viscoelastic. Mighri *et al.* (1998) experimentally observed drop deformation where drop and the matrix fluids were Boger fluids with four different relaxation times. They observed that increased drop viscoelasticity decreased drop deformation whereas increased matrix viscoelasticity enhanced it. As a result, they observed that increasing the elasticity parameter $k = \lambda_d/\lambda_m = De_d/De_m$ decreased drop deformation. Specifically, they compared the deformation of a fully elastic system with that of a fully Newtonian (N/N) system. We would further expect that for smaller k, matrix elasticity would dominate and the drop deformation would be larger than that in the fully Newtonian (N/N) system, while for larger k, the drop viscoelasticity would dominate to decrease the deformation from the N/N system. Mighri *et al.* commented that for $k < 0.37$, steady-state deformation was always greater than that for the corresponding N/N system and for $k \geqslant 0.37$ the steady-state deformation was always less than that for the N/N system. However, the experimental system used by Mighri *et al.* (1998) is such that both λ_d and λ_m are varied to arrive at different values of k rather than fixing the drop/matrix phase elasticity (De) while varying the elasticity ratio, which admittedly is difficult to achieve in an experiment. Note that the critical k value, in general, should depend on the Deborah number. In any event, following Mighri *et al.* (1998), we plot in figure 10 the steady-state deformation as a function of k for $Ca = 0.2$ for four different matrix Deborah numbers ($De_m = 0.1, 0.5, 1.0, 2.0$). The inset shows a plot of the steady-state inclination angle for the same cases. For each of the different curves, we have fixed the bulk phase elasticity and varied the drop phase elasticity. We observe, as expected, a monotonic decrease in D_{st} (and an attendant monotonic increase in φ_{st}) with k. However, note that in figure 5(*b*), we observe a non-monotonic response for the N/O case, in that for small De_m, the matrix viscoelasticity tends to decrease the deformation (as does the drop viscoelasticity). Therefore, unlike Mighri *et al.*'s results, we observe that D_{st} in the fully elastic case is lower than that of the fully Newtonian system ($D_{st} = 0.233$) for all values of k, at smaller values of De_m. However, for higher values, e.g. $De_m = 2.0$, we observe that D_{st} in the elastic system is higher than 0.233 (N/N value) for small k.

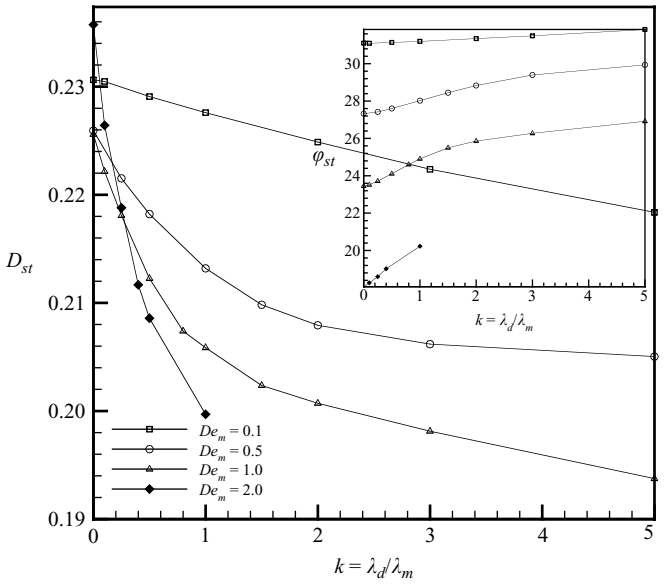

FIGURE 10. Change in steady-state drop deformation D_{st} with elasticity ratio k for different De_m values at $Ca = 0.2$. Inset shows the change in φ_{st}.

11. Summary

Following the numerical investigation of an Oldroyd-B drop deforming in a Newtonian matrix, we have presented results for the inverse problem of a Newtonian drop in an Oldroyd-B matrix. We have compared experimental observations of drop response to variation in matrix viscoelasticity. The drop inclination angle decreases because of the normal stresses in the matrix, which thereby rotates the drop away from the stretching axis. This along with a localized stretching of the polymer molecules at the drop tips causes a non-monotonic change in steady-state deformation with De. The change in orientation angle of a Newtonian drop owing to matrix phase viscoelasticity is opposite to and much more pronounced than what was observed for a viscoelastic drop in a Newtonian matrix. The viscous and viscoelastic forces are investigated in detail and shown to be in a subtle balance giving rise to the complex drop response. The angle was also shown to play a critical role in the observed non-monotonic behaviour. For breakup, at supercritical capillary numbers we see a range of De in which the matrix viscoelasticity is seen to stabilize Newtonian drops against breakup. However, above that range, matrix viscoelasticity seems to promote breakup. For fully elastic systems, we observe that the drop deformation decreases with increasing elasticity ratio, while the drop alignment decreases.

The work is partially supported by NSF grant CBET-0625599. We also thank Professor Stefano Guido for providing his experimental data.

Appendix A

Consider the single-phase steady shear flow of an Oldroyd-B fluid with polymeric viscosity μ_p. At $t = 0$, a fully developed shear flow $\boldsymbol{u}(\boldsymbol{x}, 0) = \dot{\gamma} y \hat{\boldsymbol{j}}$ and extra stress

$\boldsymbol{T}^p(\boldsymbol{x}, 0) = \boldsymbol{0}$ is assumed. The Oldroyd-B equations are

$$\lambda\left[\frac{\partial T_{xx}}{\partial t} - 2\left(T_{xx}\frac{\partial u}{\partial x} + T_{xy}\frac{\partial u}{\partial y} + T_{xx}\frac{\partial u}{\partial z}\right)\right] + T_{xx} = 0, \tag{A 1}$$

$$\lambda\frac{\partial T_{xy}}{\partial t} + T_{xy} = \mu_p\dot{\gamma} + \lambda\dot{\gamma}T_{yy}, \tag{A 2}$$

$$\lambda\frac{\partial T_{yy}}{\partial t} + T_{yy} = 0. \tag{A 3}$$

The solutions are $T_{yy} = 0$, $T_{xy}(t) = \mu_p\dot{\gamma}[1 - \exp(-t/\lambda)]$. The (x, y)-component of the extra stress contributes to an extra stress along the streamlines, although there is no straining motion in the (x, x)-direction. Thus, (A 1) reduces to

$$\lambda\frac{\partial T_{xx}}{\partial t} + T_{xx} = 2\mu_p\dot{\gamma}(\lambda\dot{\gamma})[1 - \exp(-t/\lambda)], \tag{A 4}$$

$$T_{xx}(t) = 2\mu_p\dot{\gamma}^2\lambda[1 - \exp(-t/\lambda)\{1 + t/\lambda\}].$$

The extra stress is given as

$$\boldsymbol{T}^p(\boldsymbol{x}, t) = \begin{pmatrix} 2\mu_p\dot{\gamma}^2\lambda\left\{1 - \mathrm{e}^{-t/\lambda}\left(1 + \frac{t}{\lambda}\right)\right\} & \mu_p\dot{\gamma}\left(1 - \mathrm{e}^{-t/\lambda}\right) \\ \mu_p\dot{\gamma}\left(1 - \mathrm{e}^{-t/\lambda}\right) & 0 \end{pmatrix}.$$

REFERENCES

Aggarwal, N. & Sarkar, K. 2007*a* Deformation and breakup of a viscoelastic drop in a Newtonian matrix under steady shear. *J. Fluid Mech.* **584**, 1–21.

Aggarwal, N. & Sarkar, K. 2007*b* Rheology of an emulsion of viscoelastic drops in steady shear. *J. Non-Newtonian Fluid Mech.* **150**, 19–31.

Chaffey, C. E. & Brenner, H. 1967. A second order theory for shear deformation of drops. *J. Colloid Interface Sci.* **24**, 258–269.

Chinyoka, T., Renardy, Y. Y., Renardy, A. & Khismatullin, D. B. 2005 Two-dimensional study of drop deformation under simple shear for Oldroyd-B liquids. *J. Non-Newtonian Fluid Mech.* **130**, 45–56.

Cox, R. G. 1969 The deformation of a drop in a general time-dependent fluid flow. *J. Fluid Mech.* **37**, 601–623.

Elmendorp, J. J. & Maalcke, R. J. 1985 A study on polymer blending microrheology. 1. *Polymer Engng Sci.* **25**, 1041–1047.

Flumerfelt, R. W. 1972 Drop breakup in simple shear fields of viscoelastic fluids. *Indust. Engng Chem. Fund.* **11**, 312–318.

Greco, F. 2002 Drop deformation for non-Newtonian fluids in slow flows. *J. Non-Newtonian Fluid Mech.* **107**, 111–131.

Guido, S., Simeone, M. & Greco, F. 2003 Deformation of a Newtonian drop in a viscoelastic matrix under steady shear flow – Experimental validation of slow flow theory. *J. Non-Newtonian Fluid Mech.* **114**, 65–82.

Hobbie, E. K. & Migler, K. B. 1999 Vorticity elongation in polymeric emulsions. *Phys. Rev. Lett.* **82**, 5393–5396.

Hooper, R. W., de Almeida, V. F., Macosko, C. W. & Derby, J. J. 2001 Transient polymeric drop extension and retraction in uniaxial extensional flows. *J. Non-Newtonian Fluid Mech.* **98**, 141–168.

Khismatullin, D. B., Renardy, Y. & Renardy, M. 2006 Development and implementation of VOF-PROST for 3D viscoelastic liquid–liquid simulations. *J. Non-Newtonian Fluid Mech.* **140**, 120–131.

Levitt, L., Macosko, C. W. & Pearson, S. D. 1996 Influence of normal stress difference on polymer drop deformation. *Polymer Engng Sci.* **36**, 1647–1655.

Li, X. Y. & Sarkar, K. 2005*a* Effects of inertia on the rheology of a dilute emulsion of drops in shear. *J. Rheol.* **49**, 1377–1394.

Li, X. Y. & Sarkar, K. 2005*b* Numerical investigation of the rheology of a dilute emulsion of drops in an oscillating extensional flow. *J. Non-Newtonian Fluid Mech.* **128**, 71–82.

Maffettone, P. L. & Greco, F. 2004 Ellipsoidal drop model for single drop dynamics with non-Newtonian fluids. *J. Rheol.* **48**, 83–100.

Maffettone, P. L. & Minale, M. 1998. Equation of change for ellipsoidal drops in viscous flow. *J. Non-Newtonian Fluid Mech.* **78**, 227–241.

Maffettone, P. L., Greco, F., Simeone, M. & Guido, S. 2005 Analysis of start-up dynamics of a single drop through an ellipsoidal drop model for non-Newtonian fluids. *J. Non-Newtonian Fluid Mech.* **126**, 145–151.

Mighri, F., Ajji, A. & Carreau, P. J. 1997 Influence of elastic properties on drop deformation in elongational flow. *J. Rheol.* **41**, 1183–1201.

Mighri, F., Carreau, P. J. & Ajji, A. 1998 Influence of elastic properties on drop deformation and breakup in shear flow. *J. Rheol.* **42**, 1477–1490.

Minale, M. 2004 Deformation of a non-Newtonian ellipsoidal drop in a non-Newtonian matrix: extension of Maffettone–Minale model. *J. Non-Newtonian Fluid Mech.* **123**, 151–160.

Peskin, C. 1977 Numerical analysis of blood flow in the heart. *J. Comput. Phys.* **25**, 220–252.

Pillapakkam, S. B. & Singh, P. 2001 A level-set method for computing solutions to viscoelastic two-phase flow. *J. Comput. Phys.* **174**, 552–578.

Rallison, J. M. 1984 The deformation of small viscous drops and bubbles in shear flows. *Annu. Rev. Fluid Mech.* **16**, 45–66.

Ramaswamy, S. & Leal, L. G. 1999*a* The deformation of a Newtonian drop in the uniaxial extensional flow of a viscoelastic liquid. *J. Non-Newtonian Fluid Mech.* **88**, 149–172.

Ramaswamy, S. & Leal, L. G. 1999*b* The deformation of a viscoelastic drop subjected to steady uniaxial extensional flow of a Newtonian fluid. *J. Non-Newtonian Fluid Mech.* **85**, 127–163.

Sarkar, K. & Schowalter, W. R. 2000 Deformation of a two-dimensional viscoelastic drop at non-zero Reynolds number in time-periodic extensional flows. *J. Non-Newtonian Fluid Mech.* **95**, 315–142.

Sarkar, K. & Schowalter, W. R. 2001 Deformation of a two-dimensional drop at non-zero Reynolds number in time-periodic extensional flows: numerical simulation. *J. Fluid Mech.* **436**, 177–206.

Sibillo, V., Simeone, M. & Guido, S. 2004 Break-up of a Newtonian drop in a viscoelastic matrix under simple shear flow. *Rheol. Acta* **43**, 449–456.

Stone, H. A. 1994 Dynamics of drop deformation and breakup in viscous fluids. *Annu. Rev. Fluid Mech.* **26**, 65–102.

Tagvac, T. 1972 Drop deformation and breakup in simple shear fields. PhD thesis. Chemical Engineering Department, University of Houston, Texas.

Taylor, G. I. 1932 The viscosity of a fluid containing small drops of another fluid. *Proc. R. Soc. Lond.* **138**, 41–48.

Toose, E. M., Geurts, B. J. & Kuerten, J. G. M. 1995 A boundary integral method for 2-dimensional (non)-Newtonian drops in slow viscous-flow. *J. Non-Newtonian Fluid Mech.* **60**, 129–154.

Torza, S., Mason, S. G. & Cox, R. G. 1972 Particle motions in sheared suspensions. 27. Transient and steady deformation and burst of liquid drops. *J. Colloid Interface Sci.* **38**, 395–411.

Tryggvason, G., Bunner, B., Ebrat, O. & Taubar, W. 1998 Computation of multiphase flows by a finite difference front tracking method. I. multi-fluid flows. *29th Computational Fluid Dynamics Lecture Series 1998–03*. Von Karman Institute of Fluid Dynamics, Sint-Genesius-Rode, Belgium.

Tryggvason, G., Bunner, B., Esmaeeli, A., Juric, D., Al-Rawahi, N., Taubar, W., Han, J., Nas, S. & Jan, Y. J. 2001 A front-tracking method for the computations of multiphase flow. *J. Comput. Phys.* **169**, 708–759.

Tretheway, D. C. & Leal, L. G. 2001 Deformation and relaxation of Newtonian drops in planar extensional flows of a Boger fluid. *J. Non-Newtonian Fluid Mech.* **99**, 81–108.

Tucker, C. L. & Moldenaers, P. 2002 Microstructural evolution in polymer blends. *Annu. Rev. Fluid Mech.* **34**, 177–210.

Unverdi, S. O. & Tryggvason, G. 1992 A front-tracking method for viscous, incompressible multi-fluid flows. *J. Comput. Phys.* **100**, 25–37.

Vanoene, H. 1972 Modes of dispersion of viscoelastic fluids in flow. *J. Colloid Interface Sci.* **40**, 448–467.

Yue, P. T., Feng, J. J., Liu, C. & Shen, J. 2005*a* Transient drop deformation upon start up shear in viscoelastic fluids. *Phys. Fluids* **17**, 123101.

Yue, P. T., Feng, J. J., Liu, C. & Shen, J. 2005*b* Viscoelastic effects on drop deformation in steady shear. *J. Fluid Mech.* **540**, 427–437.